# Hydrogen-Rich Gas Production by Upgrading of Biomass Pyrolysis Vapors over NiBEA Catalyst: Impact of Dealumination and Preparation Method

Jacek Grams, Robert Ryczkowski, Renata Sadek, Karolina Chalupka, Kamila Przybysz, Sandra Casale, Stanislaw Dzwigaj

energy&fuels

pubs.acs.org/EF Article

# Hydrogen-Rich Gas Production by Upgrading of Biomass Pyrolysis Vapors over NiBEA Catalyst: Impact of Dealumination and Preparation Method

Jacek Grams,* Robert Ryczkowski, Renata Sadek, Karolina Chałupka, Kamila Przybysz, Sandra Casale, and Stanislaw Dzwigaj*

Cite This: *Energy Fuels* 2020, 34, 16936−16947

Read Online

ACCESS | Metrics & More | Article Recommendations

**ABSTRACT:** The main goal of this work was to develop a highly active catalyst in lignocellulosic biomass conversion to hydrogen-rich gas. The studies were focused on the evaluation of an impact of dealumination of BEA zeolites on the catalytic performance of nickel-containing BEA zeolite catalysts in the investigated process. In order to increase an efficiency of hydrogen production, the effect of the catalyst preparation method was investigated (XRD, TEM, TPR, TPD-$NH_3$, TG-DTA-MS and BET). During catalytic activity tests, cellulose and pinewood were initially pyrolyzed at 500 °C. The formed vapors were subsequently upgraded by passing them through a catalyst bed at 700 °C. The composition of the mixture of gaseous products was analyzed using GC-MS. The obtained results showed that Ni on dealuminated SiBEA zeolite, characterized by high number of vacant T atom sites, large surface area, high contribution of micropores, and relatively small pore size, was the most active among studied catalysts. The performed research demonstrated that increased reducibility of an active phase was beneficial for the enhancement of hydrogen production. The role of acid−base and redox sites as well as the influence of the state of Ni centers on the activity of Ni-containing dealuminated and nondealuminated BEA systems was also discussed. It is worth noticing that synthesized NiBEA zeolite catalysts, contrary to reference NiZSM-5 (possessing lower surface area and pore volume, lower reducibility and larger Ni crystallites), did not lose their activity in the conversion of lignocellulosic biomass in comparison to decomposition of pure cellulose.

## 1. INTRODUCTION

Lignocellulosic biomass is an abundant, renewable energy feedstock readily available around the world. Its growing importance results from increasing demand of energy and shortage of fossil fuel reserves. One of the most promising methods of lignocellulosic biomass conversion is thermal treatment leading to the formation of $H_2$-rich gas. However, its efficiency is still unsatisfactory due to formation of a large number of undesirable products. The competitiveness of thermal conversion of biomass can be increased by the use of heterogeneous catalysts.[1]

Literature shows that nickel is one of the most active metals of high temperature decomposition of lignocellulosic feedstock.[2] Moreover, it was proved that Ni catalysts allow for efficient hydrogen production in steam reforming of various organic compounds, such as ethanol.[3−5] Nevertheless, Ni based catalysts may suffer from sintering or coke deposition leading to their deactivation during biomass conversion.[6] That is why the role of the nickel support is extremely important.[7] It affects dispersion and stability of an active metal, mechanical and thermal resistance of the catalyst, its porous structure, and the number of acid or basic sites, among others.[8] The selection of the optimal support allows for the control of catalytic performance of Ni catalyst and increase in the efficiency of biomass decomposition to $H_2$-rich gas.

At the beginning, researchers focused on the application of materials widely used as catalyst supports, such as $Al_2O_3$ (thermally resistant, facilitating dispersion of active phase),[2] $ZrO_2$ (thermally stable, possessing both acidic and basic sites,[9] limiting coke formation),[10] $TiO_2$ (known for its photocatalytic properties, used for example in selective oxidation of glucose),[11,12] or $SiO_2$ (with highly developed porous structure and limited surface acidity).[13] Moreover, it was demonstrated that the use of various silica based mesoporous materials, such as MCM-41, SBA-15, or KIT-6 may noticeably increase catalytic performance of Ni in the conversion of lignocellulosic feedstock.[14−16]

On the other hand, the literature demonstrates that zeolites exhibit catalytic activity in the discussed process. ZSM-5 is the one of the most popular among them.[17] Its high acidity enhances biomass decomposition at high temperature due to enhancement of cracking of thermal decomposition products. However, the presence of highly acidic sites may also lead to relatively fast formation of carbon deposit and catalyst deactivation.[18] ZSM-5 promotes the formation of aromatics and phenols in the mixture of products of the conversion of

Received: September 2, 2020
Revised: November 28, 2020
Published: December 8, 2020

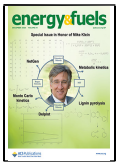

lignocellulosic feedstock, moreover deoxygenation of reaction intermediates can be enhanced.[19] Despite that its application leads to the increase in the contribution of liquid fraction reducing the volume of permanent gases. Therefore, there is a need for development of new catalysts that would increase the selectivity of biomass conversion to gaseous products, in particular to hydrogen.

One of the promising materials which can be applied as a support of Ni catalyst in thermal decomposition of lignocellulosic feedstock is BEA zeolite. It belongs to crystalline aluminosilicates, which possess a three-dimensional structure of the 12-ring pore systems. Its physicochemical properties, such as high specific surface area, well-defined porosity, and thermal stability, make it a very promising alternative to commonly used aluminum or silicon oxides.[20−22] In addition, due to the appearance of structural defects in the parent BEA zeolite network, it is possible to change its acidity through a dealumination process without damaging the framework. The use of the two-step postsynthesis method developed earlier by Dzwigaj et al.[23−25] allows for incorporation of a transition metal cation such as Ni into the framework of BEA zeolite, contributing to the emergence of new Lewis acid centers. The two-step postsynthesis method consists initially of the removal of aluminum ions from the zeolite framework by treatment with nitric acid solution. As a result, the vacant T-atom sites associated with silanol groups are created in the framework of siliceous SiBEA zeolite. In the second step, the nickel ions are incorporated in the vacant T atom sites upon contact of aqueous $Ni(NO_3)_2$ solution with SiBEA zeolite at 70 °C for 2 h. The two-step postsynthesis method ensures good dispersion of the nickel ions in the SiBEA structure allowing formation of small nickel nanoparticles upon reduction in $H_2$, in line with our earlier report.[26] Therefore, it is not surprising that NiBEA systems have been successfully applied as catalysts in various catalytic processes, such as 1,2-dichloroethane hydrodechlorination[27] or partial oxidation of methane.[26]

The authors of the reports[28−31] suggested that the use of the zeolite dealumination process allows the strength of the acidic sites to be controlled and leads to an enhancement in the availability of active sites. Moreover, Oliveira et al.[30] and Pinheiro et al.[31] indicated that the removal of aluminum atoms from the zeolite structure may contribute to the improvement of mesoporosity of the synthesized material. However, Qin et al.[28] negated this conclusion pointing to the suppressive effect of dealumination process.

Taking into account that the support of nickel catalyst for thermal conversion of lignocellulosic biomass should allow the porous network to be obtained with high surface area, thermal stability, and controlled acidity, we decided to study an impact of BEA zeolite on the catalytic performance of nickel-containing catalysts in this reaction. In order to improve the efficiency of the formation of hydrogen-rich gas, the effect of the catalyst preparation method and the zeolite dealumination process was investigated. The activity tests of the synthesized catalysts were performed for both cellulose (used as a model compound) and pine woodchips (real biomass).

## 2. EXPERIMENTAL SECTION

**2.1. Preparation of Catalysts.** Nickel-based catalysts were synthesized by conventional wet impregnation ($Ni_{20}$HAlBEA) and two-step postsynthesis methods ($Ni_{20}$SiBEA), described earlier.[32] The tetraethylammonium BEA (TEABEA) zeolites, which possess in their structure mesopores (TEABEA (I)) and micropores (TEABEA (II)) were splitted into two parts. The first part was used to obtain the organic free HAlBEA (I) (Si/Al = 18) and HAlBEA (II) (Si/Al = 21) by calcination of the parent TEABEA(I) and TEABEA(II) zeolites, respectively, at 550 °C for 15 h in air. The second fraction of the parent TEABEA(I) and TEABEA(II) zeolites was treated with 13 mol $L^{-1}$ $HNO_3$ aqueous solution to obtain SiBEA (I) (Si/Al > 1500) and SiBEA (II) (Si/Al = 669). Next, the formed nondealuminated (HAlBEA(I) and HAlBEA(II)) and dealuminated (SiBEA(I) and SiBEA(II)) zeolites were impregnated with $Ni(NO_3)_2{\cdot}6H_2O$ aqueous solution (pH 2.6−3.0) under aerobic conditions at room temperature. The obtained suspensions were stirred for 24 h at room temperature, and then, the formed solids were separated from the suspension in an evaporator under vacuum of a membrane pump for 2 h at 80 °C. Finally, the synthesized catalysts were calcined at 500 °C for 3 h in air. The obtained materials containing 20 wt % of nickel were labeled as $Ni_{20}$HAlBEA (I), $Ni_{20}$HAlBEA (II), $Ni_{20}$SiBEA (I), and $Ni_{20}$SiBEA (II), respectively. The preparation procedure of $Ni_{20}$HAlBEA and $Ni_{20}$SiBEA zeolite catalysts is identical to that described in our previous paper where the scheme of the synthesis of catalysts has been presented.[33]

$Ni_{20}$HZSM-5 catalyst was obtained by wet impregnation of HZSM-5 (Si/Al = 50) using $Ni(NO_3)_2{\cdot}6H_2O$ aqueous solution (pH 2.6−3.0) as a Ni precursor. The obtained suspension was stirred for 24 h at room temperature. Then, the separation of the solid fraction was executed in the evaporator under vacuum of a membrane pump for 2 h at 80 °C. Finally, the synthesized catalyst was calcined at 500 °C for 3 h in air. The obtained catalyst containing 20 wt % of Ni was labeled as $Ni_{20}$HZSM-5.

The catalysts subjected to characterization of their physicochemical properties in the reduced form was treated at 500 °C for 1 h in the flow of hydrogen. The activity tests were conducted in the presence of calcined catalysts, which underwent reduction in the reaction conditions.

**2.2. Characterization Methods.** The surface area of the analyzed samples was determined using ASAP2010 Micromeritics with prior outgassing of the studied materials at 200 °C for 3 h in order to desorb the impurities or moisture. The Brunauer−Emmett−Teller (BET) surface area was established using a nitrogen adsorption isotherm. The pore radius and pore volumes were calculated with the use of the t-plot method.

The X-ray diffraction patterns (XRD) were recorded with the use of Bruker D8 ADVANCE using Cu K$\alpha$ radiation ($\lambda$ = 154.05 pm) in the range of 2$\theta$ from 5 to 90° in ambient atmosphere. The size of the NiO and metallic Ni nanoparticles was calculated with the application of the Scherrer equation.

Temperature-programmed reduction measurements (TPR) were conducted with the use of AMI1 (Altamira Instruments). Before the reduction experiments, the samples were subjected to oxidation at 500 °C to remove impurities and moisture adsorbed on the sample surface. The gaseous mixture consisted of oxygen (5 vol %), and argon (95 vol %) was used in this step (flow rate 30 mL $min^{-1}$ and heating rate 20 °C $min^{-1}$). Then, the samples were cooled to ambient temperature. TPR experiments were conducted with the use of the mixture of hydrogen (5 vol %) and argon (95 vol %; ) (flow rate 30 mL $min^{-1}$ and heating rate 20 °C $min^{-1}$).

Temperature-programmed desorption of ammonia ($NH_3$-TPD) was carried out in quartz reactor. Before the adsorption of gaseous $NH_3$ (100 °C, 15 min), the samples were dried at 500 °C in He for 1 h. Next, physically adsorbed ammonia was removed from the investigated surface by the flow of He from 50 to 600 °C. The amount of $NH_3$ was monitored with the use of a thermal conductivity detector (TCD).

Transmission electron microscopy (TEM) was executed with the use of JEOL 1011 Electron Microscope. Prior the TEM measurement, a drop of suspension of catalyst, ultrasonically dispersed in pure ethanol, was deposited on the carbon film of Cu grid.

Thermogravimetric analysis (TGA-DTA-MS) was carried out with the use of derivatograph SETSYS 16/18, Setaram and mass spectrometer ThermoStar, Balzers. TGA-DTA-MS profiles were


https://dx.doi.org/10.1021/acs.energyfuels.0c02958
Energy Fuels 2020, 34, 16936−16947

Table 1. Composition of Gaseous Mixture Formed in Thermal Conversion of Cellulose

| | gas volume [ml] | $H_2$ [mmol $g^1$] | $CO_2$ [mmol $g^1$] | $CH_4$ [mmol $g^1$] | CO [mmol $g^1$] |
|---|---|---|---|---|---|
| without catalyst | 220 | 1.3 | 1.2 | 0.9 | 6.2 |
| HAlBEA (I) | 268 | 1.4 | 0.8 | 1.0 | 6.5 |
| HAlBEA (II) | 268 | 2.3 | 0.9 | 1.3 | 7.7 |
| SiBEA (I) | 262 | 1.1 | 0.8 | 1.0 | 6.7 |
| SiBEA (II) | 265 | 1.6 | 0.8 | 1.2 | 7.7 |
| HZSM-5 | 265 | 1.2 | 0.9 | 1.0 | 8.4 |
| $Ni_{20}$HAlBEA (I) | 373 | 15.8 | 3.0 | 0.8 | 8.9 |
| $Ni_{20}$HAlBEA (II) | 409 | 17.1 | 2.7 | 0.8 | 8.7 |
| $Ni_{20}$SiBEA (I) | 384 | 16.9 | 3.3 | 0.8 | 8.7 |
| $Ni_{20}$SiBEA (II) | 430 | 17.8 | 2.8 | 1.0 | 9.4 |
| $Ni_{20}$HZSM-5 | 403 | 14.8 | 2.6 | 1.0 | 9.6 |

Table 2. Composition of Gaseous Mixture Formed in Thermal Conversion of Pine Woodchips

| | gas volume [mL] | $H_2$ [mmol $g^{-1}$] | $CO_2$ [mmol $g^{-1}$] | $CH_4$ [mmol $g^{-1}$] | CO [mmol $g^{-1}$] |
|---|---|---|---|---|---|
| without catalyst | 194 | 0.8 | 0.7 | 0.9 | 7.7 |
| $Ni_{20}$HAlBEA (II) | 402 | 14.7 | 2.2 | 1.2 | 10.9 |
| $Ni_{20}$SiBEA (I) | 431 | 16.5 | 2.5 | 1.3 | 10.4 |
| $Ni_{20}$SiBEA (II) | 438 | 17.3 | 2.4 | 1.3 | 10.4 |
| $Ni_{20}$HZSM-5 | 417 | 15.9 | 2.3 | 1.3 | 10.7 |

Table 3. Physicochemical Properties of the Studied Catalysts

| | | | | | | | | acidity ($\mu$mol $g^{-1}$) | |
|---|---|---|---|---|---|---|---|---|---|
| catalyst | BET surface area [$m^2$ $g^{-1}$] | pore volume [$cm^3$ $g^{-1}$] | micropore volume ($cm^3$ $g^{-1}$) | pore radius [nm] | NiO crystallite size [nm] (XRD) | $Ni^0$ crystallite size [nm] (XRD) | $Ni^0$ crystallite size [nm] (TEM) | Calc. | Red. |
| $Ni_{20}$HAlBEA (I) | 359 | 0.33 | 0.14 | 7.6 | - | - | - | 1279 | - |
| $Ni_{20}$HAlBEA (II) | 366 | 0.23 | 0.14 | 3.3 | 16.7 | 16.6 | 28.8 | 1100 | 1147 |
| $Ni_{20}$SiBEA (I) | 343 | 0.26 | 0.13 | 7.0 | 7.6 | 5.8 | 5.5 | 337 | 488 |
| $Ni_{20}$SiBEA (II) | 419 | 0.20 | 0.17 | 4.4 | 16.2 | 17.2 | 17.2 | 482 | 610 |
| $Ni_{20}$HZSM-5 | 290 | 0.12 | 0.08 | 2.4 | 17.4 | 15.9 | 22.3 | 664 | 611 |

collected in the flow of air (40 mL $min^{-1}$) from 20 to 900 °C with a temperature ramp of 10 °C $min^{-1}$.

**2.3. Analysis of Catalytic Activity.** The catalytic performance of the studied catalysts was investigated using a two step quartz reactor. Initially, lignocellulosic feedstock was decomposed at 500 °C. Then formed vapors were passed through the catalyst bed where the upgrading process took place at 700 °C. The volume of produced gas was determined using a scaled gas capture syringe. Subsequently, gaseous products were directed to the gas chromatograph for analysis using Ar with a flow rate 15 mL $min^{-1}$. An analysis of the gas mixture was performed using GC Agilent 7820A equipped with the system containing Molsieve 5A and Porapak Q chromatographic columns. The activity tests were conducted using 0.4 g of $\alpha$-cellulose (Sigma-Aldrich, grain size ~0.2 mm) or pine woodchips (grain size ~0.5 mm) in the presence of 0.1 g of NiBEA catalysts. Pine woodchips were obtained via thermal treatment of pine wood in an autoclave at 172 °C for 4 h in the presence of NaOH (266 g $kg^{-1}$ wood) and $Na_2S$ (114 g $kg^{-1}$ wood). The pretreated biomass contained 94.3% of cellulose, 2.6% of lignin, and 2.5% of hemicellulose.

## 3. RESULTS

**3.1. Catalytic Activity of the Samples.** The first step of catalytic activity tests was focused on determination of the efficiency of high temperature decomposition of cellulose (Table 1). An analysis of the results obtained in the case of the process conducted without catalyst demonstrated formation of the lowest amount of gaseous products (220 mL) including 1.3 mmol $g^{-1}$ of $H_2$, 1.2 mmol $g^{-1}$ of $CO_2$, 0.9 mmol $g^{-1}$ of $CH_4$, and 6.2 mmol $g^{-1}$ of CO. An application of parent zeolites did not noticeably increase the efficiency of permanent gases production. Total gas volume was elevated slightly to about 262−268 mL, while the hydrogen yield varied between 1.1 mmol $g^{-1}$ in the case of SiBEA (I) and 2.3 mmol $g^{-1}$ for HAlBEA (II). The amount of other gaseous products remained at the same level in comparison to that for the noncatalytic reaction.

An introduction of Ni into the structure of zeolites resulted in the significant increase in the production of gaseous fraction (total gas volume varied from 373 to 430 mL). The highest $H_2$ yield was observed for $Ni_{20}$SiBEA (II) (17.8 mmol $g^{-1}$), followed by $Ni_{20}$HAlBEA (II) (17.1 mmol $g^{-1}$), then $Ni_{20}$SiBEA (I) (16.9 mmol $g^{-1}$) and $Ni_{20}$HAlBEA (I) (15.8 mmol $g^{-1}$). On the other hand, the lowest $H_2$ yield (14.8 mmol $g^{-1}$) was determined for the $Ni_{20}$HZSM-5 sample. An analysis of the production of other gaseous products demonstrated the increase in the yield of $CO_2$ (2.6−3.3 mmol $g^{-1}$) and CO (8.7−9.4 mmol $g^{-1}$), while the efficiency in the formation of $CH_4$ was the same (0.8−1.0 mmol $g^{-1}$) in comparison to the process conducted in the presence of parent zeolites (Table 1).

In the next step an activity of synthesized catalysts in thermal conversion of pine woodchips was studied (Table 2). It was observed that even in the case of noncatalytic reaction the efficiency of the formation of gaseous products was lower than that noticed for cellulose decomposition (total gas yield 194 mL, 0.8 mmol $g^{-1}$ $H_2$, 0.7 mmol $g^{-1}$ $CO_2$, $CH_4$ 0.9 mmol $g^{-1}$, and 7.7 mmol $g^{-1}$CO). The same phenomenon was


https://dx.doi.org/10.1021/acs.energyfuels.0c02958
Energy Fuels 2020, 34, 16936−16947

observed for catalytic process. However, the order of the activity of the catalysts was the same as in the case of cellulose decomposition ($Ni_{20}$SiBEA (II) 17.3 mmol $g^{-1}$, followed by $Ni_{20}$SiBEA (I) 16.5 mmol $g^{-1}$ and $Ni_{20}$HAlBEA (II) 14.7 mmol $g^{-1}$). It was worth noticing that a decrease in $H_2$ yield in the case of catalytic decomposition of pine woodchips was not significant and considerably lower than that observed for mesoporous silicas.[34] Moreover, a slight increase in the formation of methane and carbon oxide was simultaneously evidenced ($CH_4$ 1.2−1.3 mmol $g^{-1}$ and CO 10.4−10.9 mmol $g^{-1}$).

**3.2. Physicochemical Properties of the Investigated Catalysts.** *3.2.1. Surface Area and Porosity.* Comparison of the porosity of the prepared catalysts exhibited that the highest surface area among studied samples was observed for $Ni_{20}$SiBEA (II) (419 $m^2$ $g^{-1}$). Surface area of other catalysts supported on BEA zeolites ranged between 343 and 366 $m^2$ $g^{-1}$. Only in the case of $Ni_{20}$HZSM-5 it was slightly lower than 300 $m^2$ $g^{-1}$ (Table 3).

The highest pore volume was noticed for $Ni_{20}$HAlBEA (I) and $Ni_{20}$SiBEA (I) catalysts (0.33 and 0.26 $cm^3$ $g^{-1}$, respectively), while the lowest was noted for $Ni_{20}$HZSM-5 (0.12 $cm^3$ $g^{-1}$). The same trend was observed in the case of the pore radius, which was the largest for $Ni_{20}$HAlBEA (I) and $Ni_{20}$SiBEA (I) (7.6 and 7.0 nm, respectively) and again the smallest for $Ni_{20}$HZSM-5 (2.4 nm). Additionally, the obtained results exhibited that $Ni_{20}$SiBEA (II) possessed the highest volume of micropores (0.17 $cm^3$ $g^{-1}$) in comparison to other catalyst supported on BEA zeolites (0.13−0.14 $cm^3$ $g^{-1}$).

*3.2.2. X-ray Diffraction Measurements (XRD).* Figure 1 demonstrates the X-ray diffraction patterns of zeolites before

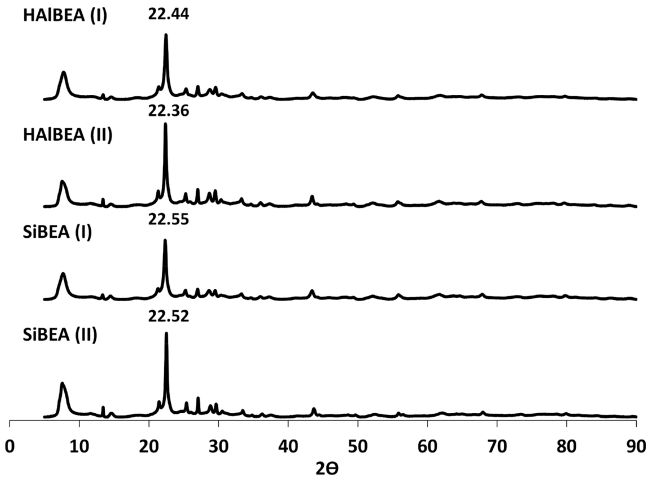


**Figure 1.** X-ray diffractograms of SiBEA(II), SiBEA(I), HAlBEA(II), and HAlBEA(I) zeolites.

the introduction of metal. In this case two major reflections at 2$\theta$ around 7.6° and 22.4° characteristic of the Beta zeolite are observed. The dealumination of HAlBEA (I) and HAlBEA (II) led to the shift of the second reflection from 22.44° and 22.36° to 22.55° and 22.52° for SiBEA (I) and SiBEA (II), respectively. The observed difference may be associated with the contraction of BEA framework, which is in line with earlier reports.[27,35] However, the crystallinity of the samples does not seem to be substantially affected during the dealumination process.[26,27,36]

An incorporation of nickel into dealuminated BEA zeolite led to the shift of the main reflection at 2$\theta$ around 22.5° to lower values, which can be related to the matrix expansion (Figure 2). However, the position of the above-mentioned

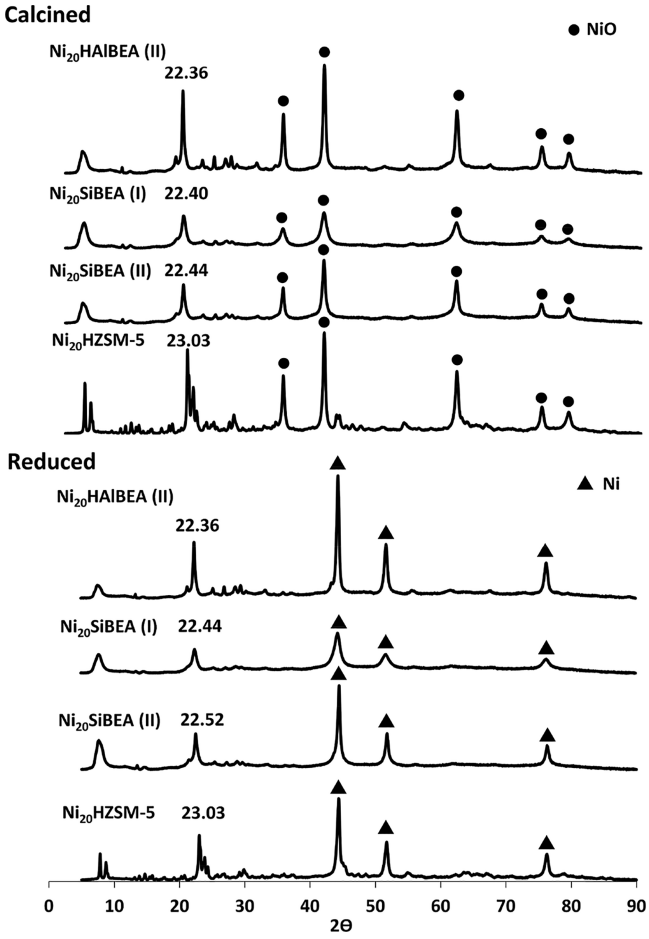


**Figure 2.** X-ray diffractograms of calcined and reduced $Ni_{20}$HZSM-5, $Ni_{20}$SiBEA(II), $Ni_{20}$SiBEA(I), and $Ni_{20}$HAlBEA(II).

reflection for $Ni_{20}$HAlBEA(II) (22.36°) is the same as that for the HAlBEA(II) support. This suggests that in the latter case nickel is not introduced into the HAlBEA(II) framework but rather remains on the surface, which is in line with earlier report.[35] On the other hand, the lack of the significant change in the intensity of the reflection at around 22.5° in the case of the reduced samples may suggest that BEA zeolite structure is stable at high temperature and does not change upon the hydrogen treatment.

The reflections at 2$\theta$ of 37.2°, 43.2°, 62.8°, 75.3°, and 79.4° observed on diffractograms of calcined catalysts proved the presence of nickel oxide phase[37] (Figure 2). The reduction of the samples in hydrogen atmosphere led to the change of the shape of XRD patterns connected with the presence of reflections at 2$\theta$ of 44.4°, 51.7°, and 76.3° characteristic for metallic Ni phase (Figure 2).[36] The calculation of the Ni crystallite size (by using Scherrer equation) revealed that in the case of $Ni_{20}$HAlBEA (II), $Ni_{20}$SiBEA (II), and $Ni_{20}$HZSM-5 nickel is present in the form of the crystallites with the size of about 16−17 nm and only for $Ni_{20}$SiBEA (I) the size of Ni grains was lower than 10 nm.


https://dx.doi.org/10.1021/acs.energyfuels.0c02958
Energy Fuels 2020, 34, 16936−16947

*3.2.3. Temperature-Programmed Reduction Studies (TPR).* TPR experiments were carried out to determine the influence of the type of the support on the reducibility of nickel oxide introduced into the catalyst structure (Figure 3). The

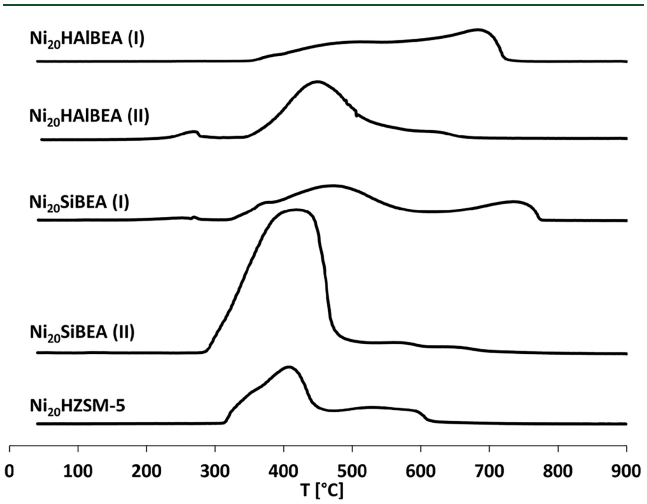


**Figure 3.** TPR profiles of $H_2$ consumption for calcined $Ni_{20}$HZSM-5, $Ni_{20}$SiBEA(II), $Ni_{20}$SiBEA(I), $Ni_{20}$HAlBEA(II), and $Ni_{20}$HAlBEA(I).

TPR profile of $Ni_{20}$HAlBEA (I) exhibits two main reduction maxima near 460 and 700 °C, indicating the presence of a strong interaction between an active phase and the support.[38] For $Ni_{20}$HAlBEA (II) only one intense maximum of hydrogen consumption near 450 °C is present. However, a small shoulder near 620 °C can be also noticed. The reduction of the major part of nickel oxide at lower temperatures suggests that the nickel oxide species are more easily reducible in the latter case.

The same trend was observed for dealuminated materials. TPR profile of $Ni_{20}$SiBEA (I) revealed two broad peaks with the maxima of hydrogen consumption near 460 and 730 °C. In the case of $Ni_{20}$SiBEA (II) the reduction of nickel oxide proceeded at lower temperatures. The maximum of the main reduction peak was recorded at 405 °C suggesting a weaker interaction betwen an active phase and SiBEA zeolite.[26] The similar reduction behavior exhibited $Ni_{20}$HZSM-5. In this case the main reduction signal with the maximum at 405 °C and less intense broad shoulder beetwen 500 and 600 °C was noticed.

Analyzing TPR profiles it can be observed that, due to high metal content (20 wt %) some part of nickel is most likely accumulated on the surface of investigated catalysts. The hydrogen uptake up to 350 °C can be associated with the reduction of extraframework NiO and/or octahedral Ni(II) species.[39,40] The presence of signals with the maxima near 450−500 °C can be linked with pseudotetrahedral Ni(II) species located in the framework of zeolite and/or oligomeric NiO,[41] while the reduction over 600 °C can be ascribed to the formation of spinel phase in the form of $NiAl_2O_4$ or $Ni_2SiO_4$.[35]

*3.2.4. Temperature-Programmed Desorption Measurements (TPD-$NH_3$).* In order to determine the acidity of the investigated materials TPD-$NH_3$ experiments were carried out (Table 4 and Figures 4 and 5). An analysis of TPD-$NH_3$ profiles obtained for pure zeolites showed the presence of peaks corresponding to weak (159−221 °C), medium (286−348 °C), and strong (381−536 °C) acid sites (Figure 4).[42,43] According to the earlier studies,[44] the low- and high-temperature signals may be related to the presence of Lewis and Brønsted acidic sites, respectively. Furthermore, some part of desorbed $NH_3$ in the low-temperature range could be ascribed to the presence of structural defects in the support structure.[45]

**Table 4. Content and Strength of Acid Sites on the Surface of Investigated Catalysts**

| | acidic sites | | | |
|---|---|---|---|---|
| sample | weak (%) | medium (%) | strong (%) | total amount of $NH_3$ ($\mu$mol $g^{-1}$) |
| HAlBEA (I) | 40 | 0 | 60 | 1629 |
| $Ni_{20}$HAlBEA (I) | 58 | 0 | 42 | 1279 |
| SiBEA (I) | 49 | 0 | 51 | 500 |
| $Ni_{20}$SiBEA (I) | 79 | 0 | 21 | 337 |
| Red-$Ni_{20}$SiBEA (I) | 58 | 29 | 13 | 488 |
| HAlBEA (II) | 39 | 0 | 61 | 1523 |
| $Ni_{20}$HAlBEA (II) | 66 | 0 | 34 | 1100 |
| Red-$Ni_{20}$HAlBEA (II) | 47 | 46 | 7 | 1147 |
| SiBEA (II) | 90 | 0 | 10 | 834 |
| $Ni_{20}$SiBEA (II) | 84 | 0 | 16 | 482 |
| Red-$Ni_{20}$SiBEA (II) | 33 | 59 | 8 | 610 |
| HZSM-5 | 53 | 0 | 47 | 1008 |
| $Ni_{20}$HZSM-5 | 48 | 34 | 18 | 664 |
| Red-$Ni_{20}$HZSM-5 | 71 | 21 | 8 | 611 |

It was demonstrated that dealumination of zeolites led to the reduction of the intensity of low- and high-temperature signals observed in TPD-$NH_3$ spectra. This phenomenon was related to the elimination of both Lewis and Brønsted acidic sites. The removal of the aluminum from the zeolite framework not only resulted in a decrease in the amount of acid sites but also shifted the high-temperature peak to higher temperature. This indicated an increase in the strength of Brønsted acidic sites remained in the structure of BEA zeolite after dealumination.[44] Furthermore, dealumination of BEA zeolite framework resulted in the shift of the peaks with the maxima at 221 and 220 °C (for HAlBEA (I) and HAlBEA (II)) to 159 and 165 °C (for SiBEA (I) and SiBEA (II), respectively). The same trend was observed by Wang et al. for H-beta zeolite.[46] This can be related to the formation of Lewis acidic sites with lower strength in the structure of the dealuminated Beta zeolite.

The $NH_3$-TPD profile of HZSM-5 exhibited ammonia desorption peaks with the maxima at 203 and 381 °C, which were ascribed to the presence of weak and strong acid sites. It can be noted that the position of the high-temperature peak for HZSM-5 was shifted toward higher temperature in comparison to the signal noticed in the case of HAlBEA. According to Hegde et al.[45] this phenomenon suggests the lower strength of acid centers in the latter case.

The ammonia desorption spectra obtained for nickel catalysts revealed the presence of weak (143−192 °C) and strong (453−529 °C) acid sites (Figure 5A). Moreover, it was demonstrated that an introduction of metal into the structure of BEA zeolite led to the shift of the maxima of low-temperature peaks toward lower temperature. This phenomenon was related to the formation of weaker Lewis acidic sites - Ni(II) species. On the other hand, one can observe that, the nickel addition into the framework of HZSM-5 and non-dealuminated BEA zeolite, resulted in the shift of the peak form medium temperature range (381 °C for HZSM-5, 330 °C for HAlBEA (II) and 348 °C for HAlBEA (I)) to high temperature range (440 °C $Ni_{20}$HZSM-5, 453 °C for


https://dx.doi.org/10.1021/acs.energyfuels.0c02958
Energy Fuels 2020, 34, 16936−16947

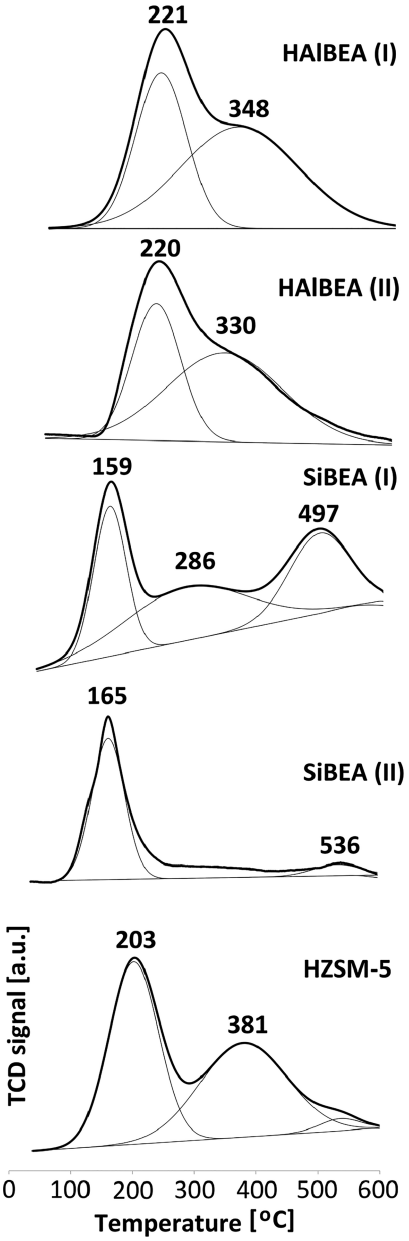


**Figure 4.** TPD-$NH_3$ profiles of HAlBEA(I), HAlBEA(II), SiBEA(I), SiBEA(II), and HZSM-5.

$Ni_{20}$HAlBEA (II) and 465 °C for $Ni_{20}$HAlBEA (I)). Phung et al.[47] related this with the formation of new "very strong" Lewis acidic sites. The higher temperature of the maxima of peaks for $Ni_{20}$SiBEA (I) (526 °C) and $Ni_{20}$SiBEA (II) (529 °C) than for non-dealuminated $Ni_{20}$HAlBEA(I) (465 °C) and $Ni_{20}$HAlBEA(II) (453 °C) systems indicates the stronger interaction of nickel with zeolite. This is probably related to better dispersion of Ni ions in SiBEA(I) and SiBEA(II) supports than in HAlBEA(I) and HAlBEA(II) ones.

Further measurements (Figure 5B) exhibited that the reduction of Ni catalysts resulted in the formation of an additional peak in the temperature range of 256−312 °C corresponding to the presence of acid sites with moderate strength, while the intensity of the high-temperature peak was lower than that observed for nonreduced samples.[39]

The quantitative results of $NH_3$-TPD measurements are presented in Table 4. Both dealuminated SiBEA (I) and SiBEA (II) supports exhibited much lower acidity (500 and 834 $\mu$mol $g^{-1}$, respectively) than corresponding nondealuminated HAlBEA (I) and HAlBEA (II)) supports (1629 and 1523 $\mu$mol $g^{-1}$, respectively), which is in agreement with the previous work.[26] Furthermore, dealumination process diminished contribution of strong acidic sites on the surface of SiBEA zeolites. The introduction of metal into the structure of HAlBEA (I), HAlBEA (II), and SiBEA (I) led to the decrease of their acidity suggesting the blockage of some number of acidic sites by nickel oxide. However, in the case of the SiBEA (II), the introduction of metal enhanced the amount of adsorbed $NH_3$. This phenomenon can be probably connected with the creation of new Ni (II) Lewis acidic sites, which was described by Chalupka et al.[26] The overall acidity of HZSM-5 (1008 $\mu$mol $g^{-1}$) is lower than that of HAlBEA (I) and HAlBEA (II). As for other catalysts an introduction of Ni on the surface of HZSM-5 resulted in the reduction of the amount of adsorbed $NH_3$.

A comparison of the strength of acid sites (Table 4) exhibited that contribution of the weak acidic sites decreased in the following order: $Ni_{20}$SiBEA (II) (84%) > $Ni_{20}$SiBEA (I) (79%) > $Ni_{20}$HAlBEA (II) (66%) > $Ni_{20}$HAlBEA (I) (58%) > $Ni_{20}$HZSM-5 (48%). Simultaneously, $Ni_{20}$SiBEA (II) possessed the lowest content of the strongest acid sites (16%). It was worth noticing that the reduction of Ni catalysts supported on BEA zeolites led to a slight increase in surface acidity and formation of a higher number of medium acid sites.

*3.2.5. Thermogravimetric Analysis (TG-DTA-MS).* TG-DTA-MS experiments were carried out in order to determine the amount and reactivity of carbon deposited on the surface of Ni-containing zeolite catalysts. The obtained results (Table 5) demonstrated that in all cases the carbon content ranged about 30 wt %. Additionally, TGA-DTA-MS spectra (Figure 6) revealed that carbon deposit removal from the surface of the tested catalysts began at about 300 °C. The highest intensity of $CO_2$ production was observed between 500 and 620 °C. The shape of the obtained profiles of carbon dioxide formation was the same for the catalysts subjected to both cellulose and pine woodchips decomposition. However, in the latter case the maximum of the $CO_2$ signal was slightly shifted toward a lower temperature (from 597 to 589 °C). This can be related with a slightly different structure of coke formed during conversion of lignocellulosic feedstock and more intense formation of carbonaceous fibers.[48] The TEM images collected from the surface of spent catalysts (subjected to cellulose conversion; Figure 7) confirmed that formed coke mainly took a shape of carbon whiskers.[49] However, the existence of some part of graphitic carbon cannot be excluded.

*3.2.6. Transmission Electron Microscopy Measurements (TEM).* TEM images and histograms demonstrating distribution of Ni nanoparticles size on the surface of the studied catalysts were shown in Figure 8. The transmission electron microscopy measurements demonstrated the lowest average size of nickel particles (5.5 nm) in the case of $Ni_{20}$SiBEA(I) which was followed by $Ni_{20}$SiBEA(II) (17.2 nm). A comparison of Ni nanoparticles existed on the surface of $Ni_{20}$SiBEA(II) and $Ni_{20}$HAlBEA(II) exhibited considerably larger Ni crystallites in the latter case (28.8 nm). This is due to the dispersion of Ni ions into vacant T-atom sites of dealuminated SiBEA zeolites during the second step of two-step postsynthesis preparation method. Simultaneously, relatively large nickel particles were noticed for $Ni_{20}$HZSM-5 (22.3 nm). It is worth mentioning that in the case of the


https://dx.doi.org/10.1021/acs.energyfuels.0c02958
Energy Fuels 2020, 34, 16936−16947

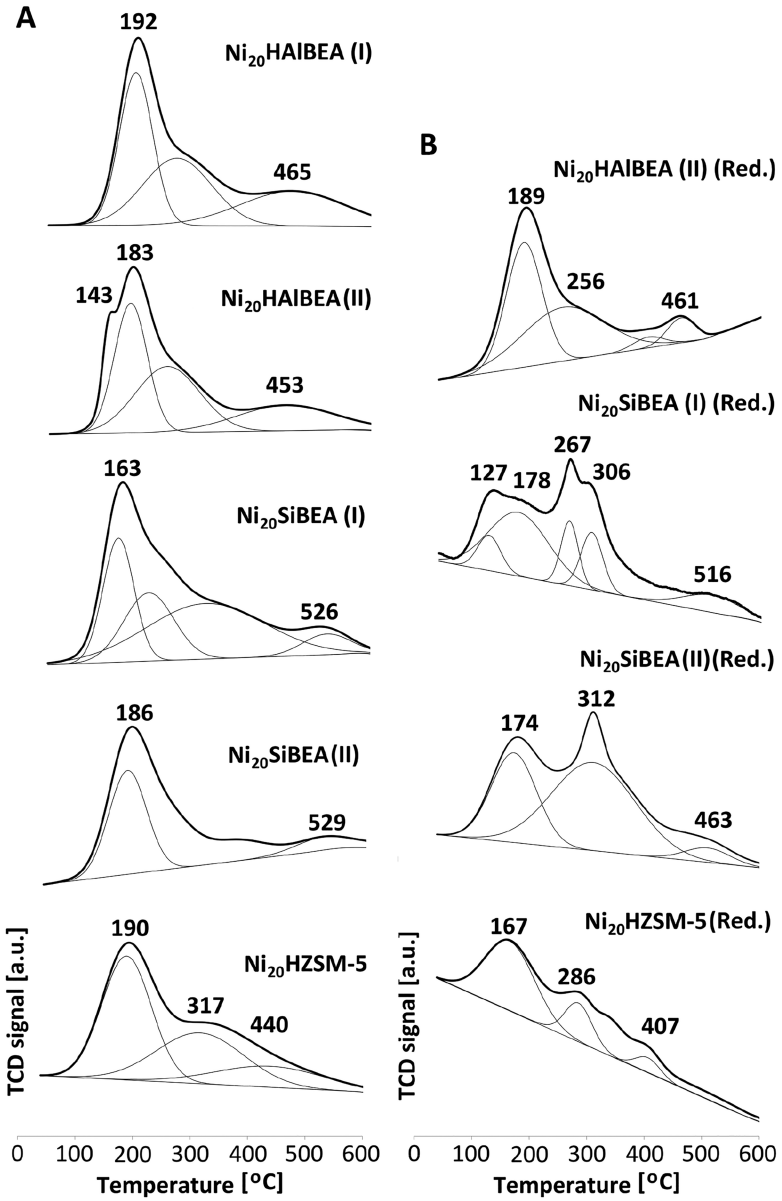


**Figure 5.** TPD-$NH_3$ profiles of the calcined (A) and reduced (B) catalysts.

**Table 5. Carbon Content on the Surface of Spent $Ni_{20}$SiBEA (I), $Ni_{20}$SiBEA (II), $Ni_{20}$HAlBEA (II), and $Ni_{20}$HZSM-5**

| | carbon deposit [wt %] | |
|---|---|---|
| catalyst | cellulose | pine |
| $Ni_{20}$SiBEA (I) | 31.5 | 34.2 |
| $Ni_{20}$SiBEA (II) | 33.1 | 26.8 |
| $Ni_{20}$HAlBEA (II) | 27.5 | 26.5 |
| $Ni_{20}$HZSM-5 | 29.2 | 30.0 |

catalysts possessing large Ni noanoparticles ($Ni_{20}$HAlBEA(II) and $Ni_{20}$HZSM-5) the higher contribution of metal agglomerates with the size exceeding 20 nm was observed.

The obtained results indicated that the two-step postsynthesis method allow to prepare the catalyst with much lower size of nickel nanoparticles. Moreover, it was demonstrated that the porous structure of the supports significantly impacted the size of formed Ni nanoparticles. $Ni_{20}$SiBEA(I) having one of the largest pore radius (7 nm) possessed the lowest average diameter of Ni particles (5.5 nm). The same tendency was observed by Bacariza et al.[50]

It is worth noticing that nickel particles could be deposited in the pores and on the surface of the zeolites. The size of nickel nanoparticles in the case of $Ni_{20}$HAlBEA(II) and $Ni_{20}$HZSM-5 measured by TEM (28.8 and 22.3 nm, respectively) was much larger than the pore radius of the supports suggesting that, during the preparation of these catalysts, an agglomeration of Ni crystallites on the surface of the support can be observed, which is in line with earlier report.[51]

## 4. DISCUSSION

The literature shows that, in the first step of thermal conversion of biomass, thermal decomposition of the feedstock is observed.[52] This leads to the formation of primary products which are subsequently subjected to depolymerization, cracking, dehydration, decarboxylation, decarbonylation, and


https://dx.doi.org/10.1021/acs.energyfuels.0c02958
Energy Fuels 2020, 34, 16936−16947

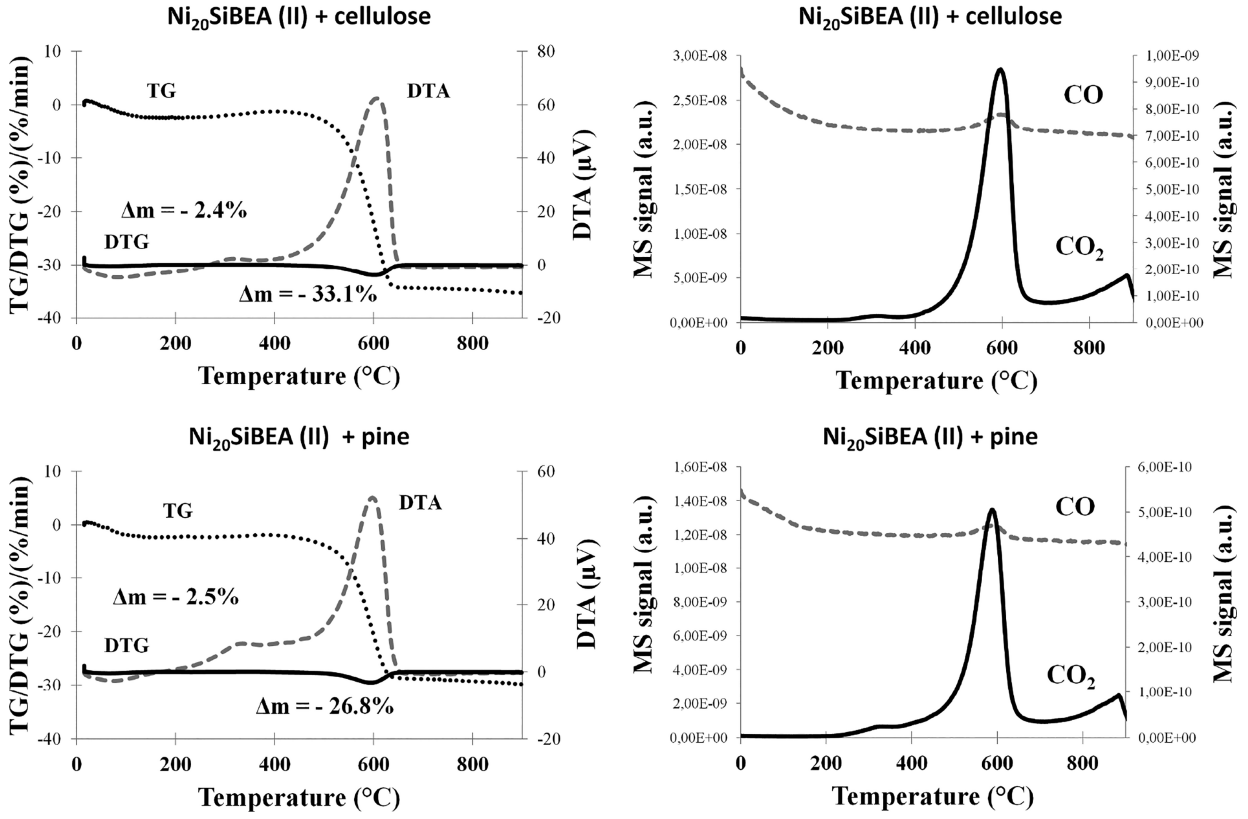


**Figure 6.** TGA-DTA-MS profiles for the $Ni_{20}$SiBEA (II) catalyst subjected to cellulose and pine woodchips decomposition.

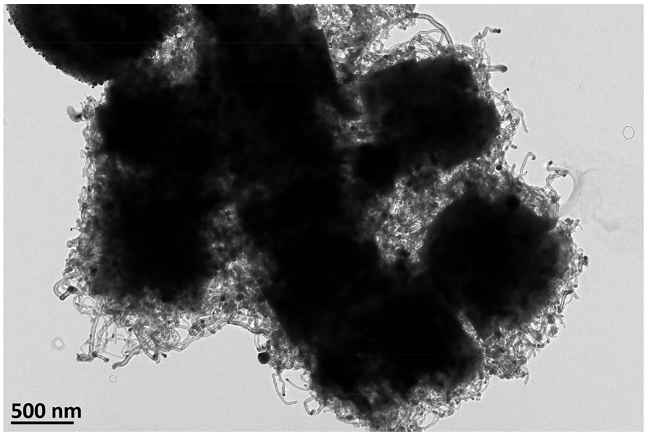


**Figure 7.** TEM image of spent $Ni_{20}$SiBEA (II) catalyst showing the growth of carbon whiskers.

elimination reactions, among others. As a consequence, noncondensable compounds, liquid fraction (mainly oxygenates), tar, and char can be formed.[53] Tanksale et al.[54] demonstrated that the mixture of gaseous products is mainly consisted of hydrogen, carbon oxide, carbon dioxide, methane, water, and light oxygenates formed in the initial step of pyrolysis (eq 1):

$$\text{lignocellulosic biomass} \rightarrow H_2 + CO + CO_2 + CH_4 + H_2O + C_nH_m + \text{oxygenates} + \text{tars} + \text{char} \quad \text{(thermal decomposition)} \tag{1}$$

The light molecules present in the gaseous phase can react with each other in the next reaction stages increasing the efficiency of hydrogen production. Methane or other light hydrocarbons interact with water molecules (coming from dehydration of biomass or moisture) at elevated temperatures which leads to formation of syngas (eqs 2 and 3, steam reforming). Methane can also react directly with carbon dioxide produced in biomass pyrolysis increasing syngas yield (eq 4, dry reforming). The $H_2$ content may be increased due to the water−gas shift reaction (eq 5) resulting in conversion of carbon oxide and water to carbon dioxide and hydrogen.

$$CH_4 + H_2O \rightarrow CO + 3H_2 \quad \text{(steam reforming)} \tag{2}$$

$$C_xH_y + xH_2O \rightarrow xCO + (x + y/2)H_2 \quad \text{(steam reforming)} \tag{3}$$

$$CH_4 + CO_2 \rightarrow 2CO + H_2 \quad \text{(dry reforming)} \tag{4}$$

$$CO + H_2O \rightarrow CO_2 + H_2 \quad \text{(water−gas shift)} \tag{5}$$

On the other hand, the amount of hydrogen can be limited by other reactions taking place, for example methanation (eq 6) consisting of the reaction between CO and $H_2$ (being syngas components) and formation of methane. Therefore, the conditions of biomass decomposition process should be strictly controlled to avoid undesirable transformation of the main reaction product.

$$CO + 3H_2 \rightarrow CH_4 + H_2O \quad \text{(methanation)} \tag{6}$$

An application of nickel catalyst in thermal conversion of lignocellulosic biomass facilitates breakdown of carbon−carbon and carbon−oxygen bonds. Becasue of that, more effective cracking, reforming, and water−gas shift can be observed. This results in the formation of a larger amount of


https://dx.doi.org/10.1021/acs.energyfuels.0c02958
Energy Fuels 2020, 34, 16936−16947

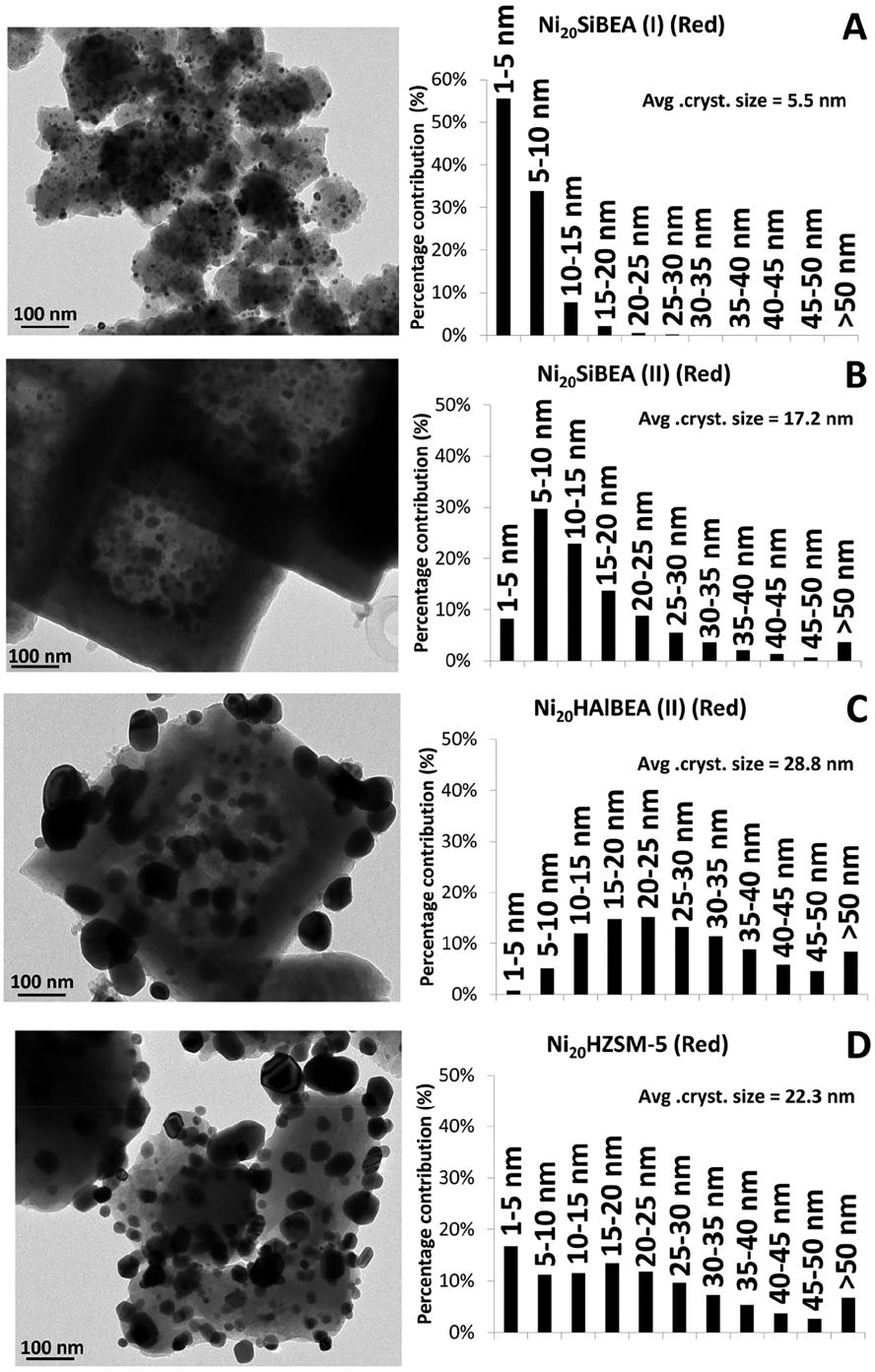


**Figure 8.** TEM images and distribution of the size of nickel crystallites on the surface of the studied catalysts.

gaseous compounds and increases the efficiency of hydrogen production.[55]

The obtained results revealed that an activity of Ni/BEA catalysts strictly depends on the support preparation method. An analysis of the porosity of the studied catalysts indicated that the materials having higher contribution of micropores and smaller pore size allowed for more efficient production of hydrogen (Table 1 and 1 vs Table 3). The most active $Ni_{20}$SiBEA (II) possessed also the highest surface area among tested materials. This may indicate that the presence of smaller pores may be responsible for reduction of distance among the active phase particles which can favor more efficient formation of simple molecules (permanent gases).[56] However, this stays in contrast with our previous research of Ni/MCF catalyst.[34] It was suggested in the latter case that larger pores enabled more efficient contact between an active phase of the catalyst and large reaction intermediates. Taking that into account, it seems that in the case of Ni/BEA besides porosity the catalyst acidity and especially reducibility of nickel oxide can affect catalytic performance to a greater extent.

A comparison of reducibility of the NiO phase supported on zeolites prepared by different methods (TPR, Figure 3) showed that the catalysts undergoing reduction at a lower temperature exhibited higher activity in lignocellulosic biomass conversion to hydrogen-rich gas ($Ni_{20}$SiBEA (II) and $Ni_{20}$HAlBEA (II) vs $Ni_{20}$SiBEA (I) and $Ni_{20}$HAlBEA (I)). In


https://dx.doi.org/10.1021/acs.energyfuels.0c02958
Energy Fuels 2020, 34, 16936−16947

this case nickel oxide can be more easily transformed to metallic nickel which strongly facilitates hydrogenation of oxygenates formed in the first step of high temperature decomposition of biomass.[57]

Temperature-programmed desorption of ammonia measurements (Table 4 and Figures 4 and 5) demonstrated the highest acidity of $Ni_{20}$HAlBEA catalysts (1100−1300 $\mu$mol $NH_3$ $g^{-1}$), while the number of acid sites observed in the case of $Ni_{20}$SiBEA was noticeably lower (300−600 $\mu$mol $NH_3$ $g^{-1}$). Moreover, $Ni_{20}$HAlBEA possessed higher contribution of strong acid sites. In spite of that their number decreased after reduction of the catalyst in hydrogen flow, it was still higher than that noticed for $Ni_{20}$SiBEA catalysts. Literature shows that higher surface acidity and higher number of strong acid sites may favor cracking of large primary products of decomposition of lignocellulosic feedstock to small molecules which should enhance the formation of gaseous compounds.[58] However, strong acid sites may undergo relatively fast deactivation due to the adsorption of carbon species which leads to a decrease in the activity of $Ni_{20}$HAlBEA in relation to that noticed for $Ni_{20}$SiBEA catalysts.[59]

An analysis of transmission electron microscopy images of $Ni_{20}$SiBEA (I) and $Ni_{20}$SiBEA (II) (Figure 8) indicates that the size of Ni nanoparticles is not a crucial factor influencing catalytic activity (5 and 17 nm, respectively). An increased reducibility of nickel oxide observed for $Ni_{20}$SiBEA (II) seems to be more beneficial. The presence of stronger interaction between nickel oxide and zeolite noticed for $Ni_{20}$SiBEA (I) decreased the efficiency of hydrogen production.

An evaluation of the effect of dealumination revealed that introduction of Ni into structure of dealuminated zeolite allowed for the increase in $H_2$ formation. First of all, it resulted from a decrease in surface acidity (TPD-$NH_3$), smaller size of Ni crystallites (TEM), and easier reducibility of nickel oxide phase (TPR) in comparison to $Ni_{20}$HAlBEA catalysts.

A comparison of catalytic performance of Ni/BEA catalysts with the activity of Ni supported on HZSM-5 confirmed that an application of BEA zeolite allows for the increase in hydrogen production (Tables 1 and 2). Hydrogen yield observed for Ni/BEA (17.8−14.7 mmol $H_2$ $g^{-1}$) was also higher than that observed for Ni supported on a commercial alumina or silica (about 10−12 mmol $H_2$ $g^{-1}$).[60,61] Moreover, the catalytic performance of the most active $Ni_{20}$SiBEA (II) was higher than that noticed for bimetallic Ni−Co catalyst supported on SBA-15 (about 13.5 mmol $H_2$ $g^{-1}$) and Ni/$CaAlO_x$ catalyst (not more than 15.6 mmol $H_2$ $g^{-1}$ depending on the contribution of Ca and Al).[62−64] It is worth mentioning that in contrast to Ni/MCF (15.9 mmol $H_2$ $g^{-1}$ in cellulose conversion and 11.0 mmol $H_2$ $g^{-1}$ in pine decomposition)[34] an activity of Ni/BEA catalysts did not noticeably change in the presence of real biomass feedstock (17.8 mmol $H_2$ $g^{-1}$ in cellulose conversion and 17.3 mmol $H_2$ $g^{-1}$ in pine decomposition in the case of $Ni_{20}$SiBEA (II)), which is certainly a promising feature of Ni supported on BEA zeolites.

## 5. CONCLUSIONS

The results of the performed studies showed that an application of Ni/BEA catalyst allows for the efficient conversion of lignocellulosic feedstock to $H_2$-rich gas. It was demonstrated that increased reducibility of an active phase resulted in the enhancement of the production of hydrogen ($Ni_{20}$SiBEA (II) vs $Ni_{20}$SiBEA (I)). This can be related to the fact that nickel oxide can be more easily transformed to metallic nickel which strongly facilitates hydrogenation of oxygenates formed in the first step of thermal decomposition of biomass. An analysis of the effect of dealumination exhibited that catalyst with a moderate number of active sites ($Ni_{20}$SiBEA (II)) was more active in the studied process than the material characterized by high acidity ($Ni_{20}$HAlBEA (II)). Additionally, the comparison of the catalytic behavior of Ni/BEA in the conversion of cellulose and pine showed that this catalyst did not lose its activity in the conversion of real biomass possessing more complex structure than model feedstock.

## AUTHOR INFORMATION


### Corresponding Authors

**Jacek Grams** − *Institute of General and Ecological Chemistry, Faculty of Chemistry, Lodz University of Technology, 90-924 Lodz, Poland*; orcid.org/0000-0002-5087-7068; Phone: +48 42 6313106; Email: jacek.grams@p.lodz.pl

**Stanislaw Dzwigaj** − *UPMC Univ Paris 06, UMR 7197, Laboratoire de Réactivité de Surface, Sorbonne Universités, F-75005 Paris, France*; Phone: + 33 1 44272113; Email: stanislaw.dzwigaj@upmc.fr

### Authors

**Robert Ryczkowski** − *Institute of General and Ecological Chemistry, Faculty of Chemistry, Lodz University of Technology, 90-924 Lodz, Poland*

**Renata Sadek** − *Institute of General and Ecological Chemistry, Faculty of Chemistry, Lodz University of Technology, 90-924 Lodz, Poland*

**Karolina Chałupka** − *Institute of General and Ecological Chemistry, Faculty of Chemistry, Lodz University of Technology, 90-924 Lodz, Poland*

**Kamila Przybysz** − *Natural Fibers Advanced Technologies, 93-322 Lodz, Poland*

**Sandra Casale** − *UPMC Univ Paris 06, UMR 7197, Laboratoire de Réactivité de Surface, Sorbonne Universités, F-75005 Paris, France*

Complete contact information is available at: https://pubs.acs.org/10.1021/acs.energyfuels.0c02958


### Notes

The authors declare no competing financial interest.

## REFERENCES


(1) Arregi, A.; Lopez, G.; Amutio, M.; Barbarias, I.; Santamaria, L.; Bilbao, J.; Olazar, M. Kinetic Study of the Catalytic Reforming of Biomass Pyrolysis Volatiles over a Commercial Ni/$Al_2O_3$ Catalyst. *Int. J. Hydrogen Energy* **2018**, *43* (27), 12023−12033.

(2) Artetxe, M.; Alvarez, J.; Nahil, M. A.; Olazar, M.; Williams, P. T. Steam Reforming of Different Biomass Tar Model Compounds over Ni/$Al_2O_3$ Catalysts. *Energy Convers. Manage.* **2017**, *136*, 119−126.

(3) Phung, T. K.; Pham, T. L. M.; Nguyen, A. N. T.; Vu, K. B.; Giang, H. N.; Nguyen, T. A.; Huynh, T. C.; Pham, H. D. Effect of Supports and Promoters on the Performance of Ni-Based Catalysts in Ethanol Steam Reforming. *Chem. Eng. Technol.* **2020**, *43* (4), 672−688.

(4) Afolabi, A. T. F.; Kechagiopoulos, P. N.; Liu, Y.; Li, C. Z. Kinetic Features of Ethanol Steam Reforming and Decomposition Using a Biochar-Supported Ni Catalyst. *Fuel Process. Technol.* **2021**, *212*, 106622.

(5) Nabgan, W.; Nabgan, B.; Tuan Abdullah, T. A.; Ngadi, N.; Jalil, A. A.; Hassan, N. S.; Izan, S. M.; Luing, W. S.; Abdullah, S. N.;

Majeed, F. S. A. Preparation and Characterization of Zeolite Beta with Low $SiO_2/Al_2O_3$ Ratio. *Int. J. Hydrogen Energy* **2020**, *45*, 119109.
(6) Santamaria, L.; Arregi, A.; Alvarez, J.; Artetxe, M.; Amutio, M.; Lopez, G.; Bilbao, J.; Olazar, M. Performance of a $Ni/ZrO_2$ Catalyst in the Steam Reforming of the Volatiles Derived from Biomass Pyrolysis. *J. Anal. Appl. Pyrolysis* **2018**, *136*, 222−231.
(7) Grams, J.; Ruppert, A. Development of Heterogeneous Catalysts for Thermo-Chemical Conversion of Lignocellulosic Biomass. *Energies* **2017**, *10* (4), 545−570.
(8) Lu, Q.; Zhang, Z. B.; Wang, X. Q.; Dong, C. Q.; Liu, Y. Q. Catalytic Upgrading of Biomass Fast Pyrolysis Vapors Using Ordered Mesoporous $ZrO_2$, $TiO_2$ and $SiO_2$. *Energy Procedia* **2014**, *61* (801), 1937−1941.
(9) Nabgan, W.; Nabgan, B.; Tuan Abdullah, T. A.; Ngadi, N.; Jalil, A. A.; Hassan, N. S.; Izan, S. M.; Luing, W. S.; Abdullah, S. N.; Majeed, F. S. A. Conversion of Polyethylene Terephthalate Plastic Waste and Phenol Steam Reforming to Hydrogen and Valuable Liquid Fuel: Synthesis Effect of $Ni\text{-}Co/ZrO_2$ Nanostructured Catalysts. *Int. J. Hydrogen Energy* **2020**, *45* (11), 6302−6317.
(10) Ruppert, A. M.; Niewiadomski, M.; Grams, J.; Kwapiński, W. Optimization of $Ni/ZrO_2$ Catalytic Performance in Thermochemical Cellulose Conversion for Enhanced Hydrogen Production. *Appl. Catal., B* **2014**, *145*, 85−90.
(11) Xu, Q.; Ma, Y.; Zhang, J.; Wang, X.; Feng, Z.; Li, C. Enhancing Hydrogen Production Activity and Suppressing CO Formation from Photocatalytic Biomass Reforming on $Pt/TiO_2$ by Optimizing Anatase-Rutile Phase Structure. *J. Catal.* **2011**, *278* (2), 329−335.
(12) Colmenares, J. C.; Magdziarz, A. Room Temperature Versatile Conversion of Biomass-Derived Compounds by Means of Supported $TiO_2$ Photocatalysts. *J. Mol. Catal. A: Chem.* **2013**, *366*, 156−162.
(13) Zhang, X.; Tang, W.; Zhang, Q.; Wang, T.; Ma, L. Hydrocarbons Production from Lignin-Derived Phenolic Compounds over $Ni/SiO_2$ Catalyst. *Energy Procedia* **2017**, *105*, 518−523.
(14) Xue, X.; Liu, Y.; Wu, L.; Pan, X.; Liang, J.; Sun, Y. Catalytic Fast Pyrolysis of Maize Straw with a Core-Shell ZSM-5@SBA-15 Catalyst for Producing Phenols and Hydrocarbons. *Bioresour. Technol.* **2019**, *289* (June), 121691.
(15) Karnjanakom, S.; Guan, G.; Asep, B.; Hao, X.; Kongparakul, S.; Samart, C.; Abudula, A. Catalytic Upgrading of Bio-Oil over Cu/MCM-41 and Cu/KIT-6 Prepared by $\beta$-Cyclodextrin-Assisted Coimpregnation Method. *J. Phys. Chem. C* **2016**, *120* (6), 3396−3407.
(16) Grams, J.; Niewiadomski, M.; Ryczkowski, R.; Ruppert, A. M.; Kwapiński, W. Activity and Characterization of Ni Catalyst Supported on $CeO_2\text{-}ZrO_2$ for Thermo-Chemical Conversion of Cellulose. *Int. J. Hydrogen Energy* **2016**, *41* (20), 8679−8687.
(17) Veses, A.; Puértolas, B.; Callén, M. S.; García, T. Catalytic Upgrading of Biomass Derived Pyrolysis Vapors over Metal-Loaded ZSM-5 Zeolites: Effect of Different Metal Cations on the Bio-Oil Final Properties. *Microporous Mesoporous Mater.* **2015**, *209*, 189−196.
(18) Wang, L.; Lei, H.; Bu, Q.; Ren, S.; Wei, Y.; Zhu, L.; Zhang, X.; Liu, Y.; Yadavalli, G.; Lee, J.; Chen, S.; Tang, J. Aromatic Hydrocarbons Production from Ex Situ Catalysis of Pyrolysis Vapor over Zinc Modified ZSM-5 in a Packed-Bed Catalysis Coupled with Microwave Pyrolysis Reactor. *Fuel* **2014**, *129*, 78−85.
(19) Che, Q.; Yang, M.; Wang, X.; Yang, Q.; Chen, Y.; Chen, X.; Chen, W.; Hu, J.; Zeng, K.; Yang, H.; Chen, H. Preparation of Mesoporous ZSM-5 Catalysts Using Green Templates and Their Performance in Biomass Catalytic Pyrolysis. *Bioresour. Technol.* **2019**, *289* (June), 121729.
(20) Zhu, Z.; Xu, H.; Jiang, J.; Wu, H.; Wu, P. Hydrophobic Nanosized All-Silica Beta Zeolite: Efficient Synthesis and Adsorption Application. *ACS Appl. Mater. Interfaces* **2017**, *9* (32), 27273−27283.
(21) Shanjiao, K.; Yanjun, G.; Tao, D.; Ying, Z.; Yanying, Z. Preparation and Characterization of Zeolite Beta with Low $SiO_2/Al_2O_3$ Ratio. *Pet. Sci.* **2007**, *4* (1), 70−74.
(22) Do Nascimento, A. R.; De Figueredo, G. P.; Silva, E. M. F.; Melo, M. A. F.; Melo, D. M. A.; De Souza, M. J. B. Synthesis, Optimization and Characterization of Zeolite Beta (BEA): Production of ZSM-5 and $NaAlSiO_4$ as Secondary Phases. *Rev. Virtual Quim.* **2017**, *9* (4), 1570−1582.
(23) Dzwigaj, S.; Matsuoka, M.; Franck, R.; Anpo, M.; Che, M. Probing Different Kinds of Vanadium Species in the VSi$\beta$ Zeolite by Diffuse Reflectance UV-Visible and Photoluminescence Spectroscopies. *J. Phys. Chem. B* **1998**, *102* (33), 6309−6312.
(24) Dzwigaj, S.; Massiani, P.; Davidson, A.; Che, M. Role of Silanol Groups in the Incorporation of V in $\beta$ Zeolite. *J. Mol. Catal. A: Chem.* **2000**, *155* (1−2), 169−182.
(25) Dzwigaj, S. Recent Advances in the Incorporation and Identification of Vanadium Species in Microporous Materials. *Curr. Opin. Solid State Mater. Sci.* **2003**, *7* (6), 461−470.
(26) Chalupka, K. A.; Jozwiak, W. K.; Rynkowski, J.; Maniukiewicz, W.; Casale, S.; Dzwigaj, S. Partial Oxidation of Methane on $Ni_xAlBEA$ and $Ni_xSiBEA$ Zeolite Catalysts: Remarkable Effect of Preparation Procedure and Ni Content. *Appl. Catal., B* **2014**, *146*, 227−236.
(27) Baran, R.; Kamińska, I. I.; Śrębowata, A.; Dzwigaj, S. Selective Hydrodechlorination of 1,2-Dichloroethane on NiSiBEA Zeolite Catalyst: Influence of the Preparation Procedure on a High Dispersion of Ni Centers. *Microporous Mesoporous Mater.* **2013**, *169*, 120−127.
(28) Qin, Z.; Shen, W.; Zhou, S.; Shen, Y.; Li, C.; Zeng, P.; Shen, B. Defect-Assisted Mesopore Formation during Y Zeolite Dealumination: The Types of Defect Matter. *Microporous Mesoporous Mater.* **2020**, *303*, 110248.
(29) Michorczyk, P.; Zeńczak-Tomera, K.; Michorczyk, B.; Węgrzyniak, A.; Basta, M.; Millot, Y.; Valentin, L.; Dzwigaj, S. Effect of Dealumination on the Catalytic Performance of Cr-Containing Beta Zeolite in Carbon Dioxide Assisted Propane Dehydrogenation. *J. CO2 Util.* **2020**, *36*, 54−63.
(30) Oliveira, A. C.; Essayem, N.; Tuel, A.; Clacens, J. M.; Tâarit, Y. B. Comparative Study of Transformation of Linear Alkanes over Modified Mordenites and Sulphated Zirconia Catalysts: Influence of the Zeolite Acidity on the Performance of n-Butane Isomerization. *J. Mol. Catal. A: Chem.* **2008**, *293* (1−2), 31−38.
(31) Pinheiro, A. N.; Valentini, A.; Sasaki, J. M.; Oliveira, A. C. Highly Stable Dealuminated Zeolite Support for the Production of Hydrogen by Dry Reforming of Methane. *Appl. Catal., A* **2009**, *355* (1−2), 156−168.
(32) Dzwigaj, S.; Peltre, M. J.; Massiani, P.; Davidson, A.; Che, M.; Dzwigaj, S.; Massiani, P.; Sen, T.; Sivasanker, S. Incorporation of Vanadium Species in a Dealuminated $\beta$ Zeolite. *Chem. Commun.* **1998**, No. 1, 87−88.
(33) Sadek, R.; Chalupka, K. A.; Mierczynski, P.; Maniukiewicz, W.; Rynkowski, J.; Gurgul, J.; Lasoń-Rydel, M.; Casale, S.; Brouri, D.; Dzwigaj, S. The Catalytic Performance of Ni-Co/Beta Zeolite Catalysts in Fischer−Tropsch Synthesis. *Catalysts* **2020**, *10* (1), 112.
(34) Grams, J.; Ryczkowski, R.; Chałupka, K.; Sobczak, I.; Rzeźnicka, I.; Przybysz, K. Impact of Support (MCF, $ZrO_2$, ZSM-5) on the Efficiency of Ni Catalyst in High-Temperature Conversion of Lignocellulosic Biomass to Hydrogen-Rich Gas. *Materials* **2019**, *12*, 3792.
(35) Penkova, A.; Dzwigaj, S.; Kefirov, W. R.; Hadjiivanov, K.; Che, M. Effect of the Preparation Method on the State of Nickel Ions in BEA Zeolites. A Study by Fourier Transform Infrared Spectroscopy of Adsorbed CO and NO, Temperature-Programmed Reduction, and X-Ray Diffraction. *J. Phys. Chem. C* **2007**, *111* (24), 8623−8631.
(36) Śrebowata, A.; Baran, R.; Łomot, D.; Lisovytskiy, D.; Onfroy, T.; Dzwigaj, S. Remarkable Effect of Postsynthesis Preparation Procedures on Catalytic Properties of Ni-Loaded BEA Zeolites in Hydrodechlorination of 1,2-Dichloroethane. *Appl. Catal., B* **2014**, *147*, 208−220.
(37) Ryczkowski, R.; Niewiadomski, M.; Michalkiewicz, B.; Skiba, E.; Ruppert, A. M.; Grams, J. Effect of Alkali and Alkaline Earth Metals Addition on $Ni/ZrO_2$ Catalyst Activity in Cellulose Conversion. *J. Therm. Anal. Calorim.* **2016**, *126* (1), 103−110.
(38) Iriondo, A.; Cambra, J. F.; Güemez, M. B.; Barrio, V. L.; Requies, J.; Sánchez-Sánchez, M. C.; Navarro, R. M. Effect of $ZrO_2$


https://dx.doi.org/10.1021/acs.energyfuels.0c02958
Energy Fuels 2020, 34, 16936−16947

addition on $Ni/Al_2O_3$ catalyst to Produce $H_2$ from Glycerol. *Int. J. Hydrogen Energy* **2012**, *37* (8), 7084−7093.
(39) Garrido Pedrosa, A. M.; Souza, M. J. B.; Melo, D. M. A.; Araujo, A. S. Cobalt and Nickel Supported on HY Zeolite: Synthesis, Characterization and Catalytic Properties. *Mater. Res. Bull.* **2006**, *41* (6), 1105−1111.
(40) Hadjiivanov, K.; Mihaylov, M.; Klissurski, D.; Stefanov, P.; Abadjieva, N.; Vassileva, E.; Mintchev, L. Characterization of $Ni/SiO_2$ Catalysts Prepared by Successive Deposition and Reduction of Ni2+ Ions. *J. Catal.* **1999**, *185* (2), 314−323.
(41) Frontera, P.; Aloise, A.; MacArio, A.; Antonucci, P. L.; Crea, F.; Giordano, G.; Nagy, J. B. Bimetallic Zeolite Catalyst for $CO_2$ Reforming of Methane. *Top. Catal.* **2010**, *53* (3−4), 265−272.
(42) Boroń, P.; Chmielarz, L.; Gurgul, J.; Łątka, K.; Gil, B.; Krafft, J. M.; Dzwigaj, S. The Influence of the Preparation Procedures on the Catalytic Activity of Fe-BEA Zeolites in SCR of NO with Ammonia and $N_2O$ Decomposition. *Catal. Today* **2014**, *235*, 210−225.
(43) Berteau, P.; Delmon, B. Modified Aluminas: Relationship Between Activity in 1-Butanol Dehydration and Acidity Measured by NH3-TPD. *Catal. Today* **1989**, *5*, 121−130.
(44) Camiloti, A. M.; Jahn, S. L.; Velasco, N. D.; Moura, L. F.; Cardoso, D. Acidity of Beta Zeolite Determined by TPD of Ammonia and Ethylbenzene Disproportionation. *Appl. Catal., A* **1999**, *182* (1), 107−113.
(45) Hegde, S.G.; Kumar, R.; Bhat, R.N.; Ratnasamy, P. Characterization of the Acidity of Zeolite Beta by FTIR. Spectroscopy and TPD of $NH_3$. *Zeolites* **1989**, *9* (3), 231−237.
(46) Wang, H.; Xin, W. Surface Acidity of H-Beta and Its Catalytic Activity for Alkylation of Benzene with Propylene. *Catal. Lett.* **2001**, *76* (3−4), 225−229.
(47) Phung, T. K.; Radikapratama, R.; Garbarino, G.; Lagazzo, A.; Riani, P.; Busca, G. Tuning of Product Selectivity in the Conversion of Ethanol to Hydrocarbons over H-ZSM-5 Based Zeolite Catalysts. *Fuel Process. Technol.* **2015**, *137* (137), 290−297.
(48) Muley, P. D.; Henkel, C.; Abdollahi, K. K.; Marculescu, C.; Boldor, D. A Critical Comparison of Pyrolysis of Cellulose, Lignin, and Pine Sawdust Using an Induction Heating Reactor. *Energy Convers. Manage.* **2016**, *117*, 273−280.
(49) Widyaningrum, R. N.; Church, T. L.; Zhao, M.; Harris, A. T. Mesocellular-Foam-Silica-Supported Ni Catalyst: Effect of Pore Size on $H_2$ Production from Cellulose Pyrolysis. *Int. J. Hydrogen Energy* **2012**, *37* (12), 9590−9601.
(50) Bacariza, M. C.; Graça, I.; Bebiano, S. S.; Lopes, J. M.; Henriques, C. Micro- and Mesoporous Supports for $CO_2$ Methanation Catalysts: A Comparison between SBA-15, MCM-41 and USY Zeolite. *Chem. Eng. Sci.* **2018**, *175*, 72−83.
(51) Wang, S.; Yin, Q.; Guo, J.; Ru, B.; Zhu, L. Improved Fischer−Tropsch Synthesis for Gasoline over Ru, Ni Promoted Co/HZSM-5 Catalysts. *Fuel* **2013**, *108*, 597−603.
(52) Navarro, R. M.; Peña, M. A.; Fierro, J. L. G. Hydrogen Production Reactions from Carbon Feedstocks: Fossil Fuels and Biomass. *Chem. Rev.* **2007**, *107* (10), 3952−3991.
(53) Bulushev, D. A.; Ross, J. R. H. Catalysis for Conversion of Biomass to Fuels via Pyrolysis and Gasification: A Review. *Catal. Today* **2011**, *171* (1), 1−13.
(54) Tanksale, A.; Beltramini, J. N.; Lu, G. Q. M. A Review of Catalytic Hydrogen Production Processes from Biomass. *Renewable Sustainable Energy Rev.* **2010**, *14* (1), 166−182.
(55) Silveira, E. B.; Rabelo-Neto, R. C.; Noronha, F. B. Steam Reforming of Toluene, Methane and Mixtures over $Ni/ZrO_2$ Catalysts. *Catal. Today* **2017**, *289*, 289−301.
(56) Subramanian, V.; Zholobenko, V. L.; Cheng, K.; Lancelot, C.; Heyte, S.; Thuriot, J.; Paul, S.; Ordomsky, V. V.; Khodakov, A. Y. The Role of Steric Effects and Acidity in the Direct Synthesis of Iso-Paraffins from Syngas on Cobalt Zeolite Catalysts. *ChemCatChem* **2016**, *8* (2), 380−389.
(57) Chen, D.; He, L. Towards an Efficient Hydrogen Production from Biomass: A Review of Processes and Materials. *ChemCatChem* **2011**, *3* (3), 490−511.
(58) Sharma, A.; Pareek, V.; Zhang, D. Biomass Pyrolysis - A Review of Modelling, Process Parameters and Catalytic Studies. *Renewable Sustainable Energy Rev.* **2015**, *50*, 1081−1096.
(59) Nagaraja, B. M.; Bulushev, D. A.; Beloshapkin, S.; Ross, J. R. H. The Effect of Potassium on the Activity and Stability of Ni-MgO-$ZrO_2$ Catalysts for the Dry Reforming of Methane to Give Synthesis Gas. *Catal. Today* **2011**, *178* (1), 132−136.
(60) Matras, J.; Niewiadomski, M.; Ruppert, A.; Grams, J. Activity of Ni Catalysts for Hydrogen Production via Biomass Pyrolysis. *Kinet. Catal.* **2012**, *53* (5), 565−569.
(61) Grams, J.; Goscianska, J.; Potrzebowska, N.; Ryczkowski, R.; Michalkiewicz, B.; Ruppert, A. M. Impact of Zr Incorporation into the Ni/AlSBA-15 Catalyst on Its Activity in Cellulose Conversion to Hydrogen-Rich Gas. *Energy Fuels* **2017**, *31*, 14089−14096.
(62) Zhao, M.; Florin, N. H.; Harris, A. T. Mesoporous Supported Cobalt Catalysts for Enhanced Hydrogen Production during Cellulose Decomposition. *Appl. Catal., B* **2010**, *97* (1−2), 142−150.
(63) Zhao, M.; Church, T. L.; Harris, A. T. SBA-15 Supported Ni-Co Bimetallic Catalysts for Enhanced Hydrogen Production during Cellulose Decomposition. *Appl. Catal., B* **2011**, *101* (3−4), 522−530.
(64) Chen, F.; Wu, C.; Dong, L.; Vassallo, A.; Williams, P. T.; Huang, J. Characteristics and Catalytic Properties of $Ni/CaAlO_x$ catalyst for Hydrogen-Enriched Syngas Production from Pyrolysis-Steam Reforming of Biomass Sawdust. *Appl. Catal., B* **2016**, *183*, 168−175.


https://dx.doi.org/10.1021/acs.energyfuels.0c02958
*Energy Fuels* 2020, 34, 16936−16947